Conjugate Gradient Parametric Detection of Multichannel Signals

CHAOSHU JIANG, Member, IEEE
HONGBIN LI, Senior Member, IEEE
Stevens Institute of Technology

MURALIDHAR RANGASWAMY, Fellow, IEEE
AFRL/RYAP

The parametric adaptive matched filter (PAMF) detector for space-time adaptive processing (STAP) detection is reexamined in this paper. Originally, the PAMF detector was introduced by using a multichannel autoregressive (AR) parametric model for the disturbance signal in STAP detection. While the parametric approach brings in benefits such as reduced training and computational requirements as compared with fully adaptive STAP detectors, the PAMF detector as a reduced-dimensional solution remains unclear. This paper employs the conjugate-gradient (CG) algorithm to solve the linear prediction problem arising in the PAMF detector. It is shown that CG yields not only a new computationally efficient implementation of the PAMF detector, a new and efficient AR model order selection method that can naturally be integrated with CG iterations, but it also offers new perspectives of PAMF as a reduced-rank subspace detector. We first consider the integration of the CG algorithm with the matched filter (MF) and parametric matched filter (PMF) when the covariance matrix of the disturbance signal is known. It is then extended to the adaptive case where the covariance matrix is estimated from training data. Important issues such as computational complexity and convergence rate are discussed. Performance of the proposed CG-PAMF detector is examined by using the KASSPER and other computer generated data.

Manuscript received April 30, 2010; revised January 14 and March 5, 2011; released for publication May 19, 2011.

IEEE Log No. T-AES/48/2/943832.

This work was supported in part by the Air Force Office of Scientific Research (AFOSR) under Grant FA9550-09-1-0310. Dr. Rangaswamy was also supported by AFOSR under Project 2311IN.

Authors' current addresses: C. Jiang, School of Electronic Engineering, University of Electronic Science and Technology of China, Chengdu, Sichuan, China, 610054; H. Li, Department of Electrical and Computer Engineering, Stevens Institute of Technology, Hoboken, NJ, 07030, E-mail: (hli@stevens.edu.); M. Rangaswamy, AFRL/RYAP, Building 620, 2241 Avionics Circle, WPAFB, OH, 45433-7132.

I. INTRODUCTION

This paper is concerned with a multichannel signal detection problem frequently encountered in phased-array radars and many other applications. With extra spatial information provided by multiple sensors, higher performance of signal detection can be achieved (than a single-sensor system), especially in detection of signals buried in a background of directional jammers and space-time correlated clutter. A widely explored technology for multichannel signal detection is space-time adaptive processing (STAP) [1], first proposed by Brennan, Reed, and Mallett [2]. Most STAP-based methods, such as the adaptive matched filter (AMF) [3] and Kelly's generalized likelihood ratio test (GLRT) [4], need to invert a large space-time covariance matrix. These methods require not only a large number of independent, identically distributed, signal-free training data to estimate the matrix, but they also incur a high computational cost for matrix estimation and inversion.

A parametric STAP detector based on a multichannel autoregressive (AR) disturbance model has been proposed for airborne radar applications [5, 6] to reduce both the training data requirement and computation load. This method is called the parametric adaptive matched filter (PAMF) [6]. While the PAMF detector has been found to yield exceptional performance with significantly reduced training and computational requirements when compared with fully adaptive STAP detectors, the connections between the PAMF and other reduced-dimensional or partially adaptive STAP detectors [1], which have similar benefits in training and complexity, remain unclear.

This paper aims to provide some insights into this problem by employing the conjugate-gradient (CG) method to solve the linear prediction problem underlying the temporal whitening phase of the PAMF detector. Our choice of the CG method is motivated by several factors. First, as will be shown, the CG algorithm naturally leads to a subspace interpretation of the PAMF detector, and offers a connection to the other reduced-rank STAP detectors. Second, the CG method is a computationally efficient algorithm to solve the linear prediction problem underlying the PAMF detector. In particular, for airborne radar applications, due to an inherent structure of the disturbance covariance matrix, the CG algorithm can usually achieve convergence using only a few iterations, thus providing significant computational saving. Third, since the disturbance covariance matrix has a block-Toeplitz (BT) matrix structure, preconditioning methods (e.g., [7], [8], [9]) can be employed, which are very effective in further speeding up the convergence rate in CG iterations, while adding up only a modest computational overhead per iteration (due to the BT structure). Finally, as a by-product,

we show that the CG algorithm also yields a new and computationally efficient AR model order selection method that can be integrated with the CG iterations.

The remainder of this paper is organized as follows. The signal detection problem is introduced in Section II. A brief review of the matched filter (MF) and parametric matched filter (PMF) detectors is provided in Section III. In Section IV the CG versions of MF (CG-MF) and PMF (CG-PMF) and a CG-based model order selection method are proposed. The convergence rate of CG in airborne radar applications, along with a preconditioned CG-PMF (PCG-PMF) detector, are also discussed there. In Section V we consider the adaptive case and present a new model order-selection CG-PAMF (OSCG-PAMF) detector, when both the AR model order and coefficients are unknown. The performance of the proposed class of CG-PMF and CG-PAMF detectors is illustrated by numerical results in Section VI. Conclusions are summarized in Section VII.

Vectors and matrices are denoted by boldface lower-case and upper-case letters, respectively. Transpose, complex conjugate and complex conjugate transpose are, respectively, represented by $(\cdot)^{\mathrm{T}}$, $(\cdot)^*$ and $(\cdot)^{\mathrm{H}}$. $\mathbb{C}$ and $\mathbb{R}$ denote the complex and real number fields. $\mathcal{CN}(\boldsymbol{\mu},\mathbf{R})$ denotes an additive multivariate Gaussian random variable with mean vector $\boldsymbol{\mu}$ and covariance matrix $\mathbf{R}$.

II. DATA MODEL

Consider a received J-channel sequence $\{\mathbf{x}(n) \mid n = 1,2,\ldots,N\}$ corrupted by a space-time correlated disturbance random process $\mathbf{c}(n)$. The detection problem involves the following binary hypotheses:

$$\begin{aligned} H_0 &: \quad \mathbf{x}(n) = \mathbf{c}(n) \\ H_1 &: \quad \mathbf{x}(n) = a\mathbf{s}(n) + \mathbf{c}(n) \end{aligned} \tag{1}$$

where $\mathbf{s}(n)$ is a known J-channel signal and a is its deterministic but unknown complex amplitude. All vectors in (1) are $J \times 1$ vectors. For convenience of later discussions, define the following vectors in descending order: $\mathbf{s} = [\mathbf{s}^{\mathrm{T}}(N), \mathbf{s}^{\mathrm{T}}(N-1), \ldots, \mathbf{s}^{\mathrm{T}}(1)]^{\mathrm{T}}$, $\mathbf{c} = [\mathbf{c}^{\mathrm{T}}(N), \mathbf{c}^{\mathrm{T}}(N-1), \ldots, \mathbf{c}^{\mathrm{T}}(1)]^{\mathrm{T}}$, $\mathbf{x} = [\mathbf{x}^{\mathrm{T}}(N), \mathbf{x}^{\mathrm{T}}(N-1), \ldots, \mathbf{x}^{\mathrm{T}}(1)]^{\mathrm{T}}$. It is standard to assume that the disturbance $\mathbf{c}$ is a Gaussian random vector with zero-mean and space-time covariance matrix $\mathbf{R}_c \in \mathbb{C}^{JN \times JN}$, while the signal vector $\mathbf{s}(n)$ is deterministic (Swerling 0 target). Based on these assumptions, $\mathbf{x} \sim \mathcal{CN}(a\mathbf{s}, \mathbf{R}_c)$, where $a = 0$ under H_0 and $a \neq 0$ under H_1.

In STAP, the signal $\mathbf{s}$ is known as the space-time steering vector:

$$\mathbf{s} = \mathbf{s}_t \otimes \mathbf{s}_s \tag{2}$$

where $\mathbf{s}_t$ and $\mathbf{s}_s$ denote the temporal steering vector and spatial steering vector, respectively, and $\otimes$ denotes the Kronecker product. For a side-looking uniform linear array (ULA), we have $\mathbf{s}_t = (1/\sqrt{N})[e^{i2\pi(N-1)f_d}, \ldots, e^{i2\pi f_d}, 1]^{\mathrm{T}}$ with a normalized Doppler frequency f_d and $\mathbf{s}_s = (1/\sqrt{J})[e^{i2\pi(J-1)f_s}, \ldots, e^{i2\pi f_s}, 1]^{\mathrm{T}}$ with a normalized spatial frequency f_s. Practically, the true disturbance covariance matrix $\mathbf{R}_c$ is unknown, and often an estimate can be obtained from the secondary data:

$$\hat{\mathbf{R}}_c = \frac{1}{K}\sum_{k=1}^{K} \mathbf{c}_k \mathbf{c}_k^{\mathrm{H}} \tag{3}$$

where $\mathbf{c}_k$, $k = 1,2,\ldots,K$, denote the secondary data vectors assumed to be signal free. According to the well-known "RMB" rule [10], we need $K \geq 2JN - 3$ so that the average output signal-to-interference-plus-noise ratio (SINR) loss caused by covariance estimation error is less than 3 dB. Detectors with an estimated covariance matrix are often called adaptive methods.

III. MF AND PMF

Assuming a known $\mathbf{R}_c$, the MF is obtained by maximizing the output SINR of a linear receiver or the generalized likelihood ratio (GLR). The test is given by (e.g., [3]):

$$\frac{|\mathbf{s}^{\mathrm{H}}\mathbf{R}_c^{-1}\mathbf{x}|^2}{\mathbf{s}^{\mathrm{H}}\mathbf{R}_c^{-1}\mathbf{s}} \underset{H_0}{\overset{H_1}{\lessgtr}} \eta_{\mathrm{MF}} \tag{4}$$

where η_{MF} is the threshold of the MF. Equation (4) is the well-known matched subspace detector for a rank-1 signal in colored noise. Consequently, it offers unbeatable performance for the detection problem considered in (1).

For ease of exposition, the MF can also be represented by using a structure of temporal whitening cascaded with spatial whitening arising from a block LDU decomposition of the disturbance covariance matrix [6]. This form of MF is given by

$$\frac{|(\mathbf{Q}^{-1/2}\mathbf{L}^{-1}\mathbf{s})^{\mathrm{H}}(\mathbf{Q}^{-1/2}\boldsymbol{\varepsilon})|^2}{(\mathbf{Q}^{-1/2}\mathbf{L}^{-1}\mathbf{s})^{\mathrm{H}}(\mathbf{Q}^{-1/2}\mathbf{L}^{-1}\mathbf{s})} = \frac{|\tilde{\mathbf{s}}^{\mathrm{H}}\boldsymbol{\nu}|^2}{\tilde{\mathbf{s}}^{\mathrm{H}}\tilde{\mathbf{s}}} \underset{H_0}{\overset{H_1}{\lessgtr}} \eta_{\mathrm{MF}} \tag{5}$$

where $\mathbf{Q} \in \mathbb{C}^{JN \times JN}$ is a block-diagonal matrix with Hermitian matrices $\mathbf{Q}(n), n = 1,2,\ldots,N$, along the main block diagonal, and $\mathbf{L} \in \mathbb{C}^{JN \times JN}$ is a lower block-triangular matrix with $J \times J$ identity matrices along the main block diagonal. Both $\mathbf{L}$ and $\mathbf{Q}$ come from a block LDU decomposition of the disturbance covariance matrix $\mathbf{R}_c = \mathbf{L}\mathbf{Q}\mathbf{L}^{\mathrm{H}}$. Finally,

$$\boldsymbol{\varepsilon}(n) = \mathbf{x}(n) - \sum_{p=1}^{(n-1)} \mathbf{A}_n^{\mathrm{H}}(p)\mathbf{x}(n-p) \tag{6}$$

$$\boldsymbol{\nu}(n) = \mathbf{Q}^{-1/2}(n)\boldsymbol{\varepsilon}(n) \tag{7}$$

$$\tilde{\mathbf{s}}(n) = \mathbf{Q}^{-1/2}(n)\left[\mathbf{s}(n) - \sum_{p=1}^{(n-1)} \mathbf{A}_n^{\mathrm{H}}(p)\mathbf{s}(n-p)\right] \tag{8}$$

where $\mathbf{A}_n^{\mathrm{H}}(p) \in \mathbb{C}^{J\times J}$ is a block element of $\mathbf{L}^{-1}$ located at the $(n-p)$th block column and the nth block row. Due to the fact that there is no performance penalty for the prewhitening of the interference [11, ch. 6], (5) is equivalent to (4).

If the disturbance $\mathbf{c}(n)$ is stationary in time, the MF can be simplified. A PMF was introduced in [6] by modeling the disturbance as a stationary Pth-order multichannel AR process. Specifically,

$$\mathbf{c}(n) = \sum_{p=1}^{P} \mathbf{A}^{\mathrm{H}}(p)\mathbf{c}(n-p) + \boldsymbol{\varepsilon}_P(n) \tag{9}$$

where $\mathbf{A}^{\mathrm{H}}(p)$, $p = 1,2,\ldots,P$, is the pth AR matrix coefficient of linear prediction, and $\boldsymbol{\varepsilon}_P(n)$ is the temporally white noise with a spatial covariance matrix $\mathbf{Q}_P$. The PMF test is given by [6]

$$\frac{\left|\sum_{n=P+1}^{N} \tilde{\mathbf{s}}_P^{\mathrm{H}}(n)\boldsymbol{\nu}_P(n)\right|^2}{\sum_{n=P+1}^{N} \tilde{\mathbf{s}}_P^{\mathrm{H}}(n)\tilde{\mathbf{s}}_P(n)} \underset{H_0}{\overset{H_1}{\lessgtr}} \eta_{\mathrm{PMF}} \tag{10}$$

where $\boldsymbol{\nu}_P(n) = \mathbf{Q}_P^{-1/2}\boldsymbol{\varepsilon}_P(n)$ and

$$\tilde{\mathbf{s}}_P(n) = \mathbf{Q}_P^{-1/2}\left[\mathbf{s}(n) - \sum_{p=1}^{P} \mathbf{A}^{\mathrm{H}}(p)\mathbf{s}(n-p)\right] \tag{11}$$

for $n = P+1,\ldots,N$. In practice, the model order P and the AR coefficients $\{\mathbf{A}(p)\}$ are unknown and hence estimated from the secondary data and/or primary data. Different estimators lead to different versions and implementations of the PAMF detector [6, 12].

IV. CG-MF AND CG-PMF

In this section we discuss alternative implementations of the MF and PMF via the CG algorithm. The resulting detectors are referred to as the CG-MF and CG-PMF detectors, respectively, for brevity. We start from the CG-MF, which also sets the basis for the CG-PMF. The latter, by assuming that the disturbance $\mathbf{c}(n)$ is temporally stationary, is a computationally simplified version of the CG-MF. The link between the PMF and CG as developed in the sequel reveals the PMF as a reduced-dimensional subspace detector. In this section we assume knowledge of the covariance matrix of the disturbance signal. An adaptive versions of the CG-PMF (i.e., CG-PAMF) is discussed in Section V.

A. Conjugate-Gradient MF

The MF detector, as shown in Section III, can be derived from a time-varying linear prediction process. Specifically, consider the problem of linearly predicting the nth sample $\mathbf{x}(n)$ under H_0 from all prior received samples $\mathbf{x}(n-1),\mathbf{x}(n-2),\ldots,\mathbf{x}(1)$ (cf. (9))

$$\mathbf{x}(n) = \mathbf{B}^{\mathrm{H}}(n)\mathbf{y}(n) + \boldsymbol{\varepsilon}(n) \tag{12}$$

where $\mathbf{B}(n) = [\mathbf{A}_n^{\mathrm{H}}(1),\mathbf{A}_n^{\mathrm{H}}(2),\ldots,\mathbf{A}_n^{\mathrm{H}}(n-1)]^{\mathrm{H}} = [\mathbf{B}_1(n),\mathbf{B}_2(n),\ldots,\mathbf{B}_J(n)] \in \mathbb{C}^{J(n-1)\times J}$ denotes the $(n-1)$st-order time-varying multichannel linear prediction filter, and $\mathbf{y}(n) = [y_n(1), y_n(2),\ldots, y_n(J(n-1)]^{\mathrm{T}} = [\mathbf{x}^{\mathrm{T}}(n-1),\mathbf{x}^{\mathrm{T}}(n-2),\ldots,\mathbf{x}^{\mathrm{T}}(1)]^{\mathrm{T}}$ contains all $n-1$ previously received data vectors. It is noted that the above time-varying linear predictor grows in its filter order or size with n. The multichannel linear predictor is equivalent to J linear predictors:

$$x_j(n) = \mathbf{B}_j^{\mathrm{H}}(n)\mathbf{y}(n) + \varepsilon_j(n), \qquad j = 1,2,\ldots,J \tag{13}$$

where $\mathbf{B}_j(n)$ is a $J(n-1)$-dimensional vector which contains the cross-channel correlation information associated with the jth channel. The optimum linear predictor can be obtained by solving the Wiener-Hopf equations:

$$\mathbf{R}_{\mathbf{y}}(n)\mathbf{B}_j(n) = \mathbf{R}_j(n), \qquad j = 1,2,\ldots,J \tag{14}$$

where $\mathbf{R}_{\mathbf{y}}(n) = E[\mathbf{y}(n)\mathbf{y}^{\mathrm{H}}(n)] \in \mathbb{C}^{J(n-1)\times J(n-1)}$ and $\mathbf{R}_j(n) = E[\mathbf{y}(n)x_j^*(n)] \in \mathbb{C}^{J(n-1)\times 1}$. Again, note that the size of the Wiener-Hopf equation grows with n.

To obtain a temporally whitened sequence $\varepsilon(n)$ for MF detection (cf. (6)), the above linear prediction process has to be performed multiple times, starting from $n = 2$ to $n = N$. For each n, we need to solve a Wiener-Hopf equation of the form of (14). While there are various solvers to the linear Wiener-Hopf equation, we consider using the CG method, which has several properties such as fast convergence, a direct link to the Krylov subspace [7], and a built-in model order selection capability. Additional remarks on such aspects are provided shortly.

The recursive procedure involved for the determination of the linear predictors is described as follows (also see (9)).

ALGORITHM

for $n = 2$ *to* N **do**

  for $j = 1$ *to* J **do**

    Initialization. Initialize the conjugate-direction vector $\mathbf{D}_{0,j}(n)$*, gradient vector* $\boldsymbol{\gamma}_{1,j}(n)$ *and initial solution* $\mathbf{B}_{0,j}(n)$*:*

$$\mathbf{D}_{1,j}(n) = -\boldsymbol{\gamma}_{1,j}(n) = \mathbf{R}_j(n) \tag{15}$$

$$\mathbf{B}_{0,j}(n) = \mathbf{0}. \tag{16}$$

    for $k = 1,2,\ldots,$ *until convergence* ($k \le J(n-1)$) **do**

      Update the step size $\alpha_{k,j}$*:*

$$\alpha_{k,j}(n) = \frac{\|\boldsymbol{\gamma}_{k,j}(n)\|^2}{\mathbf{D}_{k,j}^{\mathrm{H}}(n)\mathbf{R}_{\mathbf{y}}(n)\mathbf{D}_{k,j}(n)}. \tag{17}$$

      Update the solution $\mathbf{B}_{k,j}$*:*

$$\mathbf{B}_{k,j}(n) = \mathbf{B}_{k-1,j}(n) + \alpha_{k,j}(n)\mathbf{D}_{k,j}(n). \tag{18}$$

      Update the gradient vector $\boldsymbol{\gamma}_{k+1,j}$*:*

$$\boldsymbol{\gamma}_{k+1,j}(n) = \boldsymbol{\gamma}_{k,j}(n) + \alpha_{k,j}(n)\mathbf{R}_{\mathbf{y}}(n)\mathbf{D}_{k,j}(n). \tag{19}$$

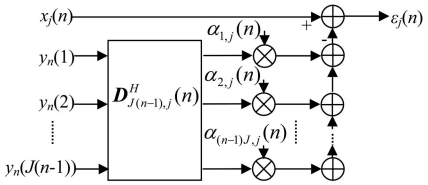

Fig. 1. Time-varying linear prediction in the CG MF detector.

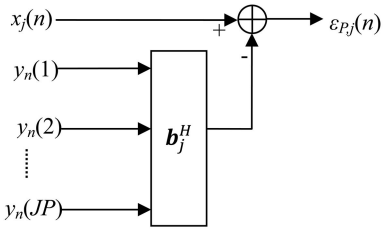

Fig. 2. Time-invariant linear prediction in the CG-PMF detector.

Update the conjugate-direction vector $\mathbf{D}_{k+1,j}$*:*

$$\mathbf{D}_{k+1,j}(n) = \mathbf{D}_{k,j}(n)\frac{\|\gamma_{k+1,j}(n)\|^2}{\|\gamma_{k,j}(n)\|^2} - \gamma_{k+1,j}(n). \tag{20}$$

end for
end for
end for

Let $\mathbf{B}(n)$ be the multichannel linear predictor formed from $\mathbf{B}_{k,j}$ after convergence. Then, $\mathbf{B}(n)$ can be used to whiten $\mathbf{x}(n)$ to produce a temporally whitened sequence $\varepsilon(n)$. The spatial covariance matrix $\mathbf{Q}(n)$ of $\varepsilon(n)$ is given by (cf. (15))

$$\begin{aligned}\mathbf{Q}(n) &= E[\varepsilon(n)\varepsilon^{\mathrm{H}}(n)] \\ &= \mathbf{R}_{\mathbf{x}}(n) - \mathbf{B}^{\mathrm{H}}(n)\mathbf{R}_{\mathbf{yx}}(n)\end{aligned} \tag{21}$$

where $\mathbf{R}_{\mathbf{x}}(n) = E[\mathbf{x}(n)\mathbf{x}^{\mathrm{H}}(n)] \in \mathbb{C}^{J\times J}$, and $\mathbf{R}_{\mathbf{yx}}(n) = E[\mathbf{y}(n)\mathbf{x}^{\mathrm{H}}(n)] \in \mathbb{C}^{J(n-1)\times J}$, which is used for further spatial whitening [6].

Fig. 1 depicts the CG-MF detector that produces the nth sample of the temporally whitened sequence $\varepsilon_j(n)$ for the jth channel, where $\mathbf{D}_{k,j}(n) = [\mathbf{D}_{1,j}(n), \mathbf{D}_{2,j}(n), \ldots, \mathbf{D}_{k,j}(n)]$ is the conjugate-direction matrix. CG iterations lead to a set of linearly independent vectors $\mathbf{D}_{1,j}(n), \ldots, \mathbf{D}_{k,j}(n)$ that are conjugate orthogonal, i.e.,

$$\mathbf{D}^{\mathrm{H}}_{k,j}(n)\mathbf{R}_{\mathbf{y}}(n)\mathbf{D}_{l,j}(n) = 0, \qquad k \neq l. \tag{22}$$

The output of the kth iteration is given by

$$\mathbf{B}_{k,j}(n) = \sum_{m=1}^{k} \alpha_{m,j}(n)\mathbf{D}_{m,j}(n) \tag{23}$$

which is a vector in the k-dimensional vector space spanned by the conjugate-direction vectors $\{\mathbf{D}_{m,j}(n), m = 1,2,\ldots,k\}$. The iterative procedure for the prediction of the nth sample $x_j(n)$, which involves a $J(n-1)$st-order linear predictor, converges after at most $J(n-1)$ iterations. The final solution $\mathbf{B}_j(n)$ lies in a $J(n-1)$-dimensional vector space.

B. CG-PMF with Known AR Model Order

If the disturbance signal can be approximated as a temporally wide-sense stationary (WSS) multichannel AR process, the linear prediction problem of the previous subsection can be significantly simplified. Specifically, suppose the disturbance is an AR(P) process with model order P. In this case the optimum linear predictor for the nth sample $\mathbf{x}(n)$ requires only P most recently received samples (as opposed to all past samples) and the prediction filter is time invariant with a fixed size (as opposed to time varying with a growing size) [13]:

$$\mathbf{x}(n) = \mathbf{B}^{\mathrm{H}}\mathbf{y}_P(n) + \varepsilon_P(n) \tag{24}$$

where the fixed Pth-order linear predictor $\mathbf{B} = [\mathbf{A}^{\mathrm{H}}(1), \mathbf{A}^{\mathrm{H}}(2), \ldots, \mathbf{A}^{\mathrm{H}}(P)]^{\mathrm{H}} = [\mathbf{B}_1, \mathbf{B}_2, \ldots, \mathbf{B}_J] \in \mathbb{C}^{JP\times J}$ is composed of the AR coefficient matrices $\{\mathbf{A}^{\mathrm{H}}(p)\}$ (cf. (9)), $\mathbf{y}_P(n) = [y_n(1), y_n(2), \ldots, y_n(JP)]^{\mathrm{T}} = [\mathbf{x}^{\mathrm{T}}(n-1), \mathbf{x}^{\mathrm{T}}(n-2), \ldots, \mathbf{x}^{\mathrm{T}}(n-P)]^{\mathrm{T}}$ denotes the regression data vector, and $n > P$. Again, it is convenient to express the above multichannel linear predictor as J scalar linear predictors:

$$x_j(n) = \mathbf{B}_j^{\mathrm{H}}\mathbf{y}_P(n) + \varepsilon_{P,j}(n), \qquad j = 1,2,\ldots,J. \tag{25}$$

The structure of temporal whitening via linear prediction for the PMF detector is shown in Fig. 2.

The solution to the scalar linear prediction problem can be obtained by solving the following Wiener-Hopf equation

$$\mathbf{R}_{\mathbf{y}}\mathbf{B}_j = \mathbf{R}_j, \qquad j = 1,2,\ldots,J \tag{26}$$

where $\mathbf{R}_{\mathbf{y}} = E[\mathbf{y}_P(n)\mathbf{y}_P^{\mathrm{H}}(n)] \in \mathbb{C}^{JP\times JP}$ and $\mathbf{R}_j = E[\mathbf{y}_P(n)x_j^*(n)] \in \mathbb{C}^{JP\times 1}$. It should be noted that unlike the MF detector, the above Wiener-Hopf is time invariant, has a fixed size, and needs to be solved only once. The resulting solution $\mathbf{B}_j$ can be used to whiten the entire received signal $\mathbf{x}(n)$ for $n > P$. The CG algorithm can also be applied to solve (26), and the resulting detector is referred to as the CG-PMF detector. Since only one fixed-sized Wiener-Hopf equation needs to be solved, the CG-PMF detector is computationally much simpler. Specifically, the outer loop for varying n as discussed in Section IVA vanishes, and only the conjugate-gradient processing with $n = P + 1$ is needed.

REMARK The iterative procedure of CG converges after at most JP iterations for the CG-PMF. As a result, the final solution $\mathbf{B}_j$ lies in a JP-dimensional vector space spanned by the conjugate-direction vectors $\mathbf{D}_{k,j}$, $k = 1,2,\ldots,JP$, or equivalently, the JP-dimensional Krylov subspace [7]:

$$\mathcal{K}(\mathbf{R}_j, \mathbf{R}_{\mathbf{y}}, JP) = \mathrm{span}\{\mathbf{R}_j, \mathbf{R}_{\mathbf{y}}\mathbf{R}_j, \ldots, \mathbf{R}_{\mathbf{y}}^{JP-1}\mathbf{R}_j\}. \tag{27}$$

This shows that the PMF is a reduced JP-dimensional solution, as opposed to the full JN-dimensional MF detector. The same conclusion applies to the adaptive version CG-PAMF detector discussed in Section V.

C. Model Order Selection by CG

In practice, the AR model order P of the disturbance is often unknown and has to be estimated. A practical approach is to choose an upper bound $\bar{P}$ for P, and use the CG algorithm to solve the following Wiener-Hopf equation

$$\mathbf{R}_{\mathbf{y}}^{(\bar{P})}\mathbf{B}_j^{(\bar{P})} = \mathbf{R}_j^{(\bar{P})}, \qquad j = 1,2,\ldots,J \tag{28}$$

where $\mathbf{R}_{\mathbf{y}}^{(\bar{P})} = E[\mathbf{y}_{\bar{P}}(n)\mathbf{y}_{\bar{P}}^{\mathrm{H}}(n)] \in \mathbb{C}^{J\bar{P}\times J\bar{P}}$ and $\mathbf{R}_j^{(\bar{P})} = E[\mathbf{y}_{\bar{P}}(n)x_j^*(n)] \in \mathbb{C}^{J\bar{P}\times 1}$. The CG iterative procedure will converge after at most $J\bar{P}$ iterations with $\mathbf{B}_j^{(\bar{P})} = [\mathbf{B}_j^{\mathrm{T}}, \mathbf{0}_{J(\bar{P}-P)\times 1}^{\mathrm{T}}]^{\mathrm{T}}$. However, with a loosely determined upper bound $\bar{P}$, it is often necessary for the sake of reducing computational complexity to stop the CG iterations before it reaches the maximum number of iterations. In this section, we propose a model order selection method for use with the CG algorithm, which is based on the following result.

LEMMA 1 *Suppose the disturbance in* (1) *is a J-channel AR(P) process. Let $\mathbf{B}_{k,j}^{(\bar{P})} \in \mathbb{C}^{J\bar{P}\times 1}$ be the solution to* (28) *obtained by CG at the kth iteration, where $k = Jp$ and $p \le \bar{P}$. Let $\mathbf{B}_j^{(p)} \in \mathbb{C}^{Jp\times 1}$ be the solution to $\mathbf{R}_{\mathbf{y}}^{(p)}\mathbf{B}_j^{(p)} = \mathbf{R}_j^{(p)}$. Then we have*

$$\mathbf{B}_{k,j}^{(\bar{P})} = \mathbf{W}_{k,j}\mathbf{B}_j^{(p)} \qquad \textit{when} \quad p = P \tag{29}$$

where $\mathbf{W}_{k,j} = \mathbf{D}_{k,j}^{(\bar{P})}\bar{\mathbf{D}}_{k,j}^{\mathrm{H}}$, $\mathbf{D}_{k,j}^{(\bar{P})} = [\mathbf{D}_{1,j}^{(\bar{P})}, \mathbf{D}_{2,j}^{(\bar{P})}, \ldots, \mathbf{D}_{k,j}^{(\bar{P})}]$ is the conjugate-direction matrix, and $\bar{\mathbf{D}}_{k,j}$ is a $k \times k$ matrix composed of the first k rows of $\tilde{\mathbf{D}}_{k,j} = [\tilde{\mathbf{D}}_{1,j}, \tilde{\mathbf{D}}_{2,j}, \ldots, \tilde{\mathbf{D}}_{k,j}]$ with

$$\tilde{\mathbf{D}}_{k,j} = \frac{\mathbf{R}_{\mathbf{y}}^{(\bar{P})}\mathbf{D}_{k,j}^{(\bar{P})}}{\mathbf{D}_{k,j}^{(\bar{P})H}\mathbf{R}_{\mathbf{y}}^{(\bar{P})}\mathbf{D}_{k,j}^{(\bar{P})}} \tag{30}$$

PROOF See Appendix I.

From (29), when $p = P$, the $J\bar{P} \times JP$ matrix $\mathbf{W}_{JP,j}$ transforms $\mathbf{B}_j$ in $\mathcal{K}(\mathbf{R}_j, \mathbf{R}_{\mathbf{y}}, JP)$, which is generated by CG-PMF with a known P, to $\mathbf{B}_{JP,j}^{(\bar{P})}$ in $\mathcal{K}(\mathbf{R}_j, \mathbf{R}_{\mathbf{y}}^{(\bar{P})}, JP)$, which is generated by CG-PMF with an unknown P. So the PMF AR coefficient vector $\mathbf{B}_j$ is completely determined by the truncated solution $\mathbf{B}_{JP,j}^{(\bar{P})}$ of CG with an unknown P after JP iterations.

We now explain how to use Lemma 1 for AR model order selection in CG-PMF. Define the residue vector

$$\boldsymbol{\epsilon}_{k,j} = \mathbf{B}_{k,j}^{(\bar{P})} - \mathbf{D}_{k,j}^{(\bar{P})}\bar{\mathbf{D}}_{k,j}^{\mathrm{H}}\mathbf{B}_j^{(p)} \qquad \text{for} \quad k = Jp. \tag{31}$$

According to (29), $\boldsymbol{\epsilon}_{k,j} = \mathbf{0}$ when $k = JP$, so the norm of $\boldsymbol{\epsilon}_{k,j}$ can be used for model order selection. However, since the Wiener solution $\mathbf{B}_j^{(p)}$ is practically unknown, $\boldsymbol{\epsilon}_{k,j}$ cannot be directly computed from (31). We propose an approach to replace $\mathbf{B}_j^{(p)}$ in (31) by the truncated solution composed of the first k elements of $\mathbf{B}_{k,j}^{(\bar{P})}$, which can be considered as an approximation of $[\mathbf{B}_j^{\mathrm{T}}, \mathbf{0}_{J(\bar{P}-P)\times 1}^{\mathrm{T}}]^{\mathrm{T}}$

$$\hat{\boldsymbol{\epsilon}}_{k,j} = \mathbf{B}_{k,j}^{(\bar{P})} - \mathbf{D}_{k,j}^{(\bar{P})}\bar{\mathbf{D}}_{k,j}^{\mathrm{H}}\bar{\mathbf{B}}_{k,j}^{(\bar{P})} \tag{32}$$

where $\bar{\mathbf{B}}_{k,j}^{(\bar{P})}$ contains the first $k = Jp$ elements of $\mathbf{B}_{k,j}^{(\bar{P})}$. Our CG-based model order selection procedure is summarized as follows.

Step 1 Select an upper bound $\bar{P}$ for the model order. One such an upper bound suggested in [6] for STAP detection is

$$\bar{P} = \max\left\{\left\lfloor \frac{3\sqrt{N}}{J} \right\rfloor\right\} \tag{33}$$

where $\lfloor\cdot\rfloor$ rounds a real-valued number towards zero.

Step 2 Use the CG algorithm to solve the Wiener-Hopf equation (28).

Step 2.1 Following every J iterations of the CG algorithm, compute the average residue over J channels:

$$\bar{\hat{\epsilon}}_k^2 = \frac{1}{J}\sum_{j=1}^{J}\|\hat{\boldsymbol{\epsilon}}_{k,j}\|^2, \qquad k = J, 2J, \ldots \tag{34}$$

Step 2.2 If $\bar{\hat{\epsilon}}_{Jp}^2$ is smaller than a specified tolerance level, then stop the CG iteration, and the estimated AR model order is $\hat{P} = p$.

The advantage of the above CG-based model order selection method is that it does not require full iterations of the CG algorithm and is efficient. The complexity of the CG algorithm with full iterations is in the same order as that of computing the inverse of $\mathbf{R}_{\mathbf{y}}^{(\bar{P})}$, which is $\mathcal{O}(J^3\bar{P}^3)$, while the complexity of using the CG-based order selection method, is $\mathcal{O}(J^3P\bar{P}^2)$. This is because the latter only requires JP iterations to determine the model order, and the additional complexity in each J iterations for (32) is the complexity of two matrix-vector multiplications, which is $2(J\bar{P})^2$. So the total complexity is $\mathcal{O}(JP(J\bar{P})^2 + 2P(J\bar{P})^2) \approx \mathcal{O}(J^3P\bar{P}^2)$. Next, we compare the computational complexity of the CG-PMF with an unknown P with the complexity of the eigencanceler [14], which is a standard eigen-subspace detector. The eigencanceler method, has a complexity of $9J^3N^3$ by using the symmetric QR algorithm to obtain the eigen-subspace and its corresponding eigenvalues [7]. Since $\bar{P} \le N$, and generally $P \ll N$, the complexity of CG-PMF is much lower than eigencanceler.

D. Convergence in Airborne Radar Applications

One important property of the CG algorithm is its fast convergence. In general, it takes no more than JP iterations to solve the linear equation (26) [7]. Even faster convergence is possible if the covariance matrix of the disturbance has some specific structure. In particular, if the covariance matrix is a rank-r_c correction of an identity matrix:

$$\mathbf{R}_y = \mathbf{R}_i + \sigma_n^2 \mathbf{I} \tag{35}$$

where $\mathbf{R}_i$ is a rank-r_c positive semidefinite matrix, then the CG algorithm converges in at most $r_c + 1$ iterations [7].

In airborne radar applications, the disturbance covariance matrix often consists of two components, namely a low-rank $\mathbf{R}_i$ due to the clutter and jamming and a scaled identity $\sigma_n^2\mathbf{I}$ due to the white noise, where σ_n^2 denotes the noise variance. The rank r_c is typically much smaller than the joint spatio-temporal dimension JN. Specifically, if the disturbance is primarily due to ground clutter and thermal noise, then according to Brennan's rule [2], the rank of the clutter covariance matrix for the full-dimensional MF is approximately

$$r_{c,\text{full}} \approx \lceil J + (N-1)\beta \rceil \tag{36}$$

where $\beta = 2v_g T_r/d$, v_g is the platform velocity, T_r is the pulse repetition period, d is the antenna element spacing, and $\lceil \cdot \rceil$ rounds a real-valued number towards infinity.

Likewise, we can approximate the rank of the disturbance covariance matrix for the PMF detector as

$$r_c \approx \lceil J + (P-1)\beta \rceil. \tag{37}$$

The smaller rank r_c over (36) is due to the fact that the disturbance covariance matrix is formed over P pulses, which is sufficient for the reduced-dimensional PMF detector due to the underlying AR(P) model. Meanwhile, the space-time disturbance covariance matrix for the full-dimensional MF detector is formed over N (the entire number of) pulses. As such, the PMF can benefit more from the fast convergence property of the CG algorithm.

E. Preconditioned CG-PMF

In cases where the disturbance covariance does not have a low-rank structure as in (35), preconditioning is usually helpful in improving the convergence rate. The idea is based on the fact that the convergence rate of CG is determined mainly by the eigenvalue structure of $\mathbf{R}_y$. In particular, the residue between the Wiener solution and kth-step CG result is bounded by [7]

$$\|\mathbf{B}_{k,j} - \mathbf{B}_j\|_{\mathbf{R}_y} \le 2\|\mathbf{B}_{0,j} - \mathbf{B}_j\|_{\mathbf{R}_y} \left(\frac{\sqrt{\kappa}-1}{\sqrt{\kappa}+1}\right)^k \tag{38}$$

where $\|\omega\|_{\mathbf{R}_y} = \sqrt{\omega^H \mathbf{R}_y \omega}$ denotes the $\mathbf{R}_y$ norm and κ is the condition number of $\mathbf{R}_y$. It is clear that rapid convergence can be achieved if κ is near 1. In the following we discuss the use of preconditioning with the CG-PMF. For simplicity, the resulting detector is referred to as the PCG-PMF detector.

Specifically, consider the modified Wiener-Hopf equation (cf. (26))

$$\tilde{\mathbf{R}}_y \tilde{\mathbf{B}}_j = \tilde{\mathbf{R}}_j \tag{39}$$

where $\tilde{\mathbf{R}}_y = \mathbf{M}^{-1/2}\mathbf{R}_y\mathbf{M}^{-1/2}$, $\tilde{\mathbf{B}}_j = \mathbf{M}^{1/2}\mathbf{B}_j$, $\tilde{\mathbf{R}}_j = \mathbf{M}^{-1/2}\mathbf{B}_j$, and $\mathbf{M}$ is a Hermitian positive-definite matrix that is called preconditioner [7]. The preconditioner is used to yield a better conditioned $\tilde{\mathbf{R}}_y$, which has a smaller condition number than $\mathbf{R}_y$, and thus a faster convergence rate. For PMF, the disturbance covariance matrix is a BT matrix. For such matrices, block-circulant (BC) preconditioners are often recommended [8, 9]. Our BC preconditioner can be directly computed from the disturbance covariance matrix $\mathbf{R}_y$ which has the following BT matrix structure:

$$\mathbf{R}_y = \begin{bmatrix} \mathbf{R}_x(0) & \cdots & \mathbf{R}_x(P-1) \\ \vdots & \ddots & \vdots \\ \mathbf{R}_x(1-P) & \cdots & \mathbf{R}_x(0) \end{bmatrix} \tag{40}$$

where $\mathbf{R}_x(m) = E[\mathbf{x}(n)\mathbf{x}^H(n-m)] \in \mathbb{C}^{J\times J}$. In particular, the BC preconditioner is given by [15]

$$\mathbf{M} = \begin{bmatrix} \mathbf{M}_0 & \mathbf{M}_{P-1} & \cdots & \mathbf{M}_1 \\ \mathbf{M}_1 & \mathbf{M}_0 & \cdots & \mathbf{M}_2 \\ \vdots & \vdots & \ddots & \vdots \\ \mathbf{M}_{P-1} & \mathbf{M}_{P-2} & \cdots & \mathbf{M}_0 \end{bmatrix}$$

where

$$\mathbf{M}_k = \frac{(P-k)\mathbf{R}_x(k) + k\mathbf{R}_x(k-P)}{P}, \qquad 0 \le k < P. \tag{41}$$

It is noted that, as shown in [7], practically $\mathbf{M}^{-1/2}$ does not need to be explicitly calculated in the PCG algorithm. The PCG algorithm is summarized as follows.

ALGORITHM

Initialization. Initialize the conjugate-direction vector $\mathbf{D}_{1,j}$, *gradient vector* $\gamma_{1,j}$, *preconditioned vector* $\mathbf{z}_{1,j}$ *and initial solution* $\mathbf{B}_{0,j}$:

$$\gamma_{1,j} = -\mathbf{R}_j \tag{42}$$

$$\mathbf{D}_{1,j} = \mathbf{z}_{1,j} = \mathbf{M}^{-1}\gamma_{1,j} \tag{43}$$

$$\mathbf{B}_{0,j} = \mathbf{0}. \tag{44}$$

for $k = 1,2,\ldots,$ *until convergence* $(k \le J(P-1))$ **do**

TABLE I
Complexity of PCG-PMF

Equation	Flops	Remark
(41)	$\mathcal{O}(J^2P)$	calculated once
$\mathbf{M}^{-1}$	$\mathcal{O}(J^2P\log_2 P + J^3P)$	calculated once
(45)	$\mathcal{O}(J^3P\log_2 P)$	at kth iteration
(46)	$\mathcal{O}(J^2P)$	at kth iteration
(47)	$\mathcal{O}(J^2P)$	at kth iteration
(48)	$\mathcal{O}(J^3P\log_2 P)$	at kth iteration
(49)	$\mathcal{O}(J^2P)$	at kth iteration
Total	$\approx \mathcal{O}(rJ^3P\log_2 P)$	for r iterations

Update the step size $\alpha_{k,j}$:

$$\alpha_{k,j} = \frac{\boldsymbol{\gamma}_{k,j}^{\mathrm{H}}\mathbf{z}_{k,j}}{\mathbf{D}_{k,j}^{\mathrm{H}}\mathbf{R}_{\mathbf{y}}\mathbf{D}_{k,j}}. \tag{45}$$

Update the solution $\mathbf{B}_{k,j}$:

$$\mathbf{B}_{k,j} = \mathbf{B}_{k-1,j} + \alpha_{k,j}\mathbf{D}_{k,j}. \tag{46}$$

Update the gradient vector $\boldsymbol{\gamma}_{k+1,j}$:

$$\boldsymbol{\gamma}_{k+1,j} = \boldsymbol{\gamma}_{k,j} + \alpha_{k,j}\mathbf{R}_{\mathbf{y}}\mathbf{D}_{k,j}. \tag{47}$$

Update the preconditioned vector $\mathbf{z}_{k+1,j}$:

$$\mathbf{z}_{k+1,j} = \mathbf{M}^{-1}\boldsymbol{\gamma}_{k+1,j}. \tag{48}$$

Update the conjugate-direction vector $\mathbf{D}_{k+1,j}$

$$\mathbf{D}_{k+1,j} = \mathbf{z}_{k,j} + \frac{\boldsymbol{\gamma}_{k+1,j}^{\mathrm{H}}\mathbf{z}_{k+1,j}}{\boldsymbol{\gamma}_{k,j}^{\mathrm{H}}\mathbf{z}_{k,j}}\mathbf{D}_{k,j}. \tag{49}$$

end for

The complexity associated with the AR parameter estimation in PCG-PMF is summarized in Table I, where r is the number of iterations needed by the PCG algorithm to reach convergence, and the flop counts are for all J channels. It is interesting to note that the PCG-PMF is computationally very efficient, involving approximately $\mathcal{O}(rJ^3P\log_2 P)$. The computational efficiency is primarily due to the fast convergence rate offered by preconditioning and the use of a BC preconditioner, as explained next. In the following we discuss the complexity of only $\mathbf{M}^{-1}$, (45), and (48), since the other calculations are obvious.

First, we consider $\mathbf{M}^{-1}$. Since $\mathbf{M}$ is a BC matrix, the inverse of $\mathbf{M}$ can be computed by using the fast Fourier transform (FFT) [16]

$$\mathbf{M}^{-1} = \begin{bmatrix} \mathbf{C}_0 & \mathbf{C}_{P-1} & \cdots & \mathbf{C}_1 \\ \mathbf{C}_1 & \mathbf{C}_0 & \cdots & \mathbf{C}_2 \\ \vdots & \vdots & \cdots & \vdots \\ \mathbf{C}_{P-1} & \mathbf{C}_{P-2} & \cdots & \mathbf{C}_0 \end{bmatrix} \tag{50}$$

where

$$\mathbf{C}_m = \frac{1}{P^2}\sum_{k=0}^{P-1} W_P^{-km}\mathbf{M}_k^{-1}, \qquad m = 0,1,\ldots,P-1 \tag{51}$$

and $W_P^{-km} = \exp(j2km\pi/P)$. It follows that the computation of $\mathbf{M}^{-1}$ is composed of P matrix inversions of $J \times J$ matrices and J^2 FFTs of length P. Therefore, the total complexity is $\mathcal{O}(J^2P\log_2 P + J^3P)$.

Second, we consider (45). The main complexity of (45) is matrix-vector multiplication $\mathbf{R}_{\mathbf{y}}\mathbf{D}_{k,j}$. Since $\mathbf{R}_{\mathbf{y}}$ is a JP-dimensional BT matrix, the above matrix-vector multiplication consists of J^2 Toeplitz matrix-vector multiplications, where each Toeplitz matrix is a $P \times P$ matrix. Each Toeplitz matrix-vector multiplication can be implemented by the FFT using $\mathcal{O}(P\log_2 P)$ flops [17]. Hence, the complexity of (45) for each channel per iteration is $\mathcal{O}(J^2P\log_2 P)$. With J channels and r iterations, the total complexity of (45) is $\mathcal{O}(rJ^3P\log_2 P)$.

Finally, we consider (48). Since the preconditioner $\mathbf{M}$ is a BC matrix, (48) can again be computed by J^2 FFTs of length P. The complexity for each channel per iteration is $\mathcal{O}(J^2P\log_2 P)$, so the total complexity of (48) for J channels is $\mathcal{O}(rJ^3P\log_2 P)$.

Here, we make a comparison between the PCG-PMF and CG-PMF. Since the condition number of the preconditioned disturbance covariance matrix $\tilde{\mathbf{R}}_{\mathbf{y}}$ is generally smaller than that of $\mathbf{R}_{\mathbf{y}}$, PCG-PMF provides a faster convergence than CG-PMF. The latter has a complexity of $\mathcal{O}(J^3P^3)$.

V. CONJUGATE-GRADIENT PAMF

The CG-PMF algorithm is now extended to the adaptive case when both the covariance matrix and the AR model order P are unknown. The resulting detector is referred to as the CG-PAMF detector. The extension of CG-PMF involves 1) replacing the true covariance matrices with estimates obtained from the target-free training data, and 2) integrating the CG-based model order selection proposed in Section IVC with CG iterations. The CG-PAMF detector with OSCG-PAMF is summarized next.

Step 1 Estimate the disturbance covariance matrices from the training data via temporal and range averaging:

$$\hat{\mathbf{R}}_{\mathbf{y}}^{(\bar{P})} = \begin{bmatrix} \hat{\mathbf{R}}_{\mathbf{x}}(0) & \cdots & \hat{\mathbf{R}}_{\mathbf{x}}(\bar{P}-1) \\ \vdots & \ddots & \vdots \\ \hat{\mathbf{R}}_{\mathbf{x}}(1-\bar{P}) & \cdots & \hat{\mathbf{R}}_{\mathbf{x}}(0) \end{bmatrix} \tag{52}$$

$$\hat{\mathbf{R}}_{\mathbf{yx}}^{(\bar{P})} = \begin{bmatrix} \hat{\mathbf{R}}_{\mathbf{x}}(-1) \\ \vdots \\ \hat{\mathbf{R}}_{\mathbf{x}}(-\bar{P}) \end{bmatrix} \tag{53}$$

where the submatrices are given by

$$\hat{\mathbf{R}}_{\mathbf{xx}}^{\mathrm{H}}(m) = \frac{1}{NK}\sum_{k=1}^{K}\sum_{l=1}^{N-m}\mathbf{x}_k(l+m)\mathbf{x}_k^{\mathrm{H}}(l) \tag{54}$$

with K denoting the number of training data vectors and $\bar{P}$ determined by (33).

Step 2 Use the CG algorithm to solve

$$\hat{\mathbf{R}}_{\mathbf{y}}^{(\bar{P})}\hat{\mathbf{B}}^{(\bar{P})} = \hat{\mathbf{R}}_{\mathbf{yx}}^{(\bar{P})}. \tag{55}$$

Step 2.1 Examine the residual $\bar{\hat{\epsilon}}_{Jp}$ (34) at each Jpth ($p = 1,2,\ldots,\bar{P}$) iteration of CG. If $\bar{\hat{\epsilon}}_{Jp} < \alpha_0\bar{\hat{\epsilon}}_{J(p-1)}$, where $0 < \alpha_0 < 1$ is a stopping threshold, then exit the CG iteration, and set the AR model order as $\hat{P} = p$.

Unlike the original PAMF with an unknown AR model order [6], which has to run recursively from $p = 1$ to a $\hat{P}$ ($\hat{P} \le \bar{P}$) to jointly estimate the AR coefficients and model order, OSCG-PAMF does not contain any recursion. It only has to perform CG with the disturbance covariance matrix $\mathbf{R}_{\mathbf{y}}^{(\bar{P})}$ for $J\hat{P}$ iterations to obtain a model order estimate.

REMARK Several estimators can be employed to find the linear prediction filters for the PAMF. The estimator as represented by (55) along with the covariance matrix estimates (52)–(54) is often called the multichannel Yule-Walker method. Other estimators, such as the least-squares estimators [6], solve slightly modified versions of the linear equation (55). It is noted that in most cases, the CG algorithm can be used to efficiently solve such a modified linear equation. Due to space limit, we do not explore these alternative CG-PAMF detectors.

A similar comparison can be made between the complexity of the OSCG-PAMF detector and that of the eigencanceler when the covariance matrix is unknown. In addition to the numbers of flops as summarized in Section IVC, both have to pay the extra complexity needed to estimate the covariance matrix. In this case, the OSCG-PAMF requires an additional complexity of $\mathcal{O}(J^2\bar{P}NK)$ as incurred in (52)–(54), whereas the extra complexity for the eigencanceler is $\mathcal{O}(J^2N^2K)$ that is used to estimate a full $(JN \times JN)$ space-time covariance matrix from K training signals.

VI. NUMERICAL RESULTS

In this section simulation results are provided to illustrate the performance of the proposed techniques. We consider simulated data generated using AR models and the KASSPER data [18], which were obtained from more realistic clutter models. The simulation results presented below use 20000 independent Monte Carlo data realizations and a probability of false alarm of $P_{\mathrm{fa}} = 10^{-2}$. The chosen P_{fa} may be considered too high for many practical detection applications. It is noted that the choice is only to facilitate computer simulation and reduce simulation time. The main observations from the simulation, including the convergence of the CG algorithm in PAMF detection and the accuracy of the estimated P provided by the proposed model order selection method, are independent of the choice of P_{fa}.

A major issue that we like to illustrate in the following numerical examples is the convergence of the CG algorithm, with partial or full iterations, when the data covariance matrix is known or estimated, and/or when the AR model order is known or estimated. To this end we compare the various detectors used with the CG algorithm, including the CG-PMF (Section IVB), CG-PAMF with a known AR model order (Section V) and OSCG-PAMF with an estimated model order (Section V), with the same detectors used with direct matrix inverse (DMI). For example, the DMI-PAMF detector involves a direct inverse of the estimated covariance matrix in (52) and uses it compute the linear prediction filter (26). This DMI approach turns out to coincide with the Yule-Walker method [13] for AR spectral estimation. It is noted in [6] that there are alternative spectral estimation methods which may yield better detection performance in some scenarios. These alternatives are not considered here since the focus is the convergence of the CG algorithm in PAMF. In the following we primarily use, as a comparison metric, the probability of detection versus the SINR for a given probability of false alarm. The output SINR of the PAMF detector was derived and extensively studied in [19].

First, we examine the performance of the two implementations of the PMF detector by using simulated data with AR disturbances. The disturbance is an AR(2) process with $J = 4$ elements and $N = 64$ pulses. Both PMF detectors have knowledge of the exact disturbance covariance matrix; however, they use different approaches to compute the linear predictor. Specifically, we consider the DMI-PMF, which uses DMI to solve the Wiener-Hopf equation, and the CG-PMF as discussed in Section IVB with knowledge of the AR model order P. The numerical results are shown in Fig. 3. It is seen that both implementations yield an identical detection performance.

We next examine the performance of the CG-based AR model order selection method used in the CG-PMF and CG-PAMF detectors with an unknown AR model order. Two AR disturbance signals with $J = 4$ and $N = 64$ are considered, and their model orders are $P = 1$ and 3, respectively. We choose the same upper bound $\bar{P} = 6$ for both cases. The residual $\bar{\hat{\epsilon}}_k$ (34) is computed and used for model order selection; as a benchmark, we also include $\bar{\epsilon}_k$, which is similarly computed as in (34) but with $\hat{\boldsymbol{\epsilon}}_{k,j}$ replaced by $\boldsymbol{\epsilon}_{k,j}$. Recall that $\bar{\hat{\epsilon}}_k$ is an approximation of $\bar{\epsilon}_k$, which cannot be computed in practice due to the fact that the

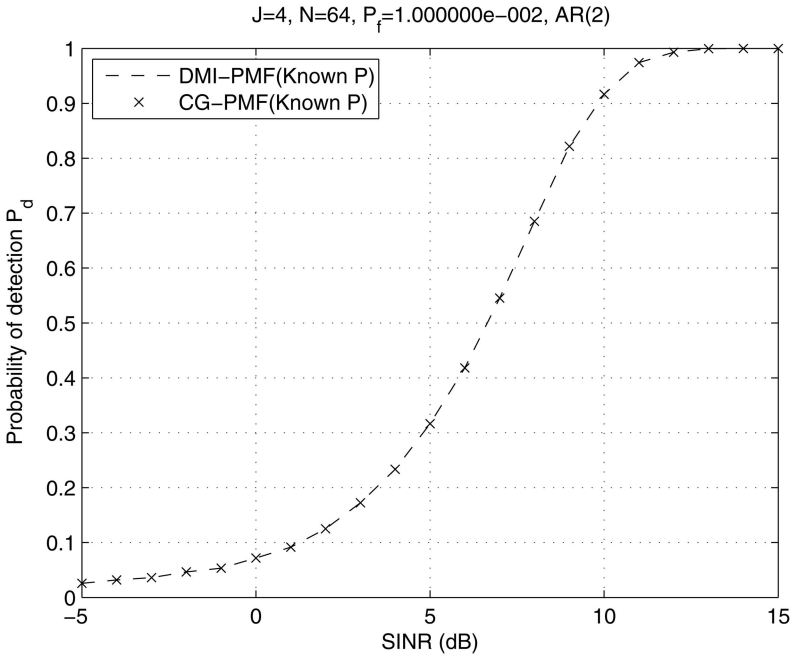

Fig. 3. Probability of detection versus SINR of PMF for simulated data($J = 4$; $N = 64$; $P = 2$).

true Wiener-Hopf solution is unknown. The numerical results for CG-PMF are shown in Fig. 4 and Fig. 5, which correspond to $P = 1$ and $P = 3$, respectively. It is seen that $\bar{\hat{\epsilon}}_k$ has a sharp decrease at the JPth ($JP = 4$ for $P = 1$ and $JP = 12$ for $P = 3$) iteration of CG, which confirms the effectiveness of the CG-based model order selection method. The counterpart model order selection results for CG-PAMF are shown in Fig. 6 and Fig. 7, for $P = 1$ and $P = 3$, respectively. Unlike the CG-PMF which uses the real disturbance covariance matrix, the sample covariance matrix estimated from the training data (cf. (40)) is employed for model order selection in CG-PAMF. Here the training data size is set to $K = 32$. It is also shown that $\bar{\hat{\epsilon}}_k$ has a sharp decrease at the JPth ($JP = 4$ for $P = 1$ and $JP = 12$ for $P = 3$) iteration of CG, although the decrease in residue is smaller than that of CG-PMF due to estimation error of the sample covariance matrix.

We now consider the convergence of PCG-PMF. The simulated disturbance is an AR(8) multichannel process with $J = 4$. The convergence of CG-PMF and PCG-PMF is shown in Fig. 8. The condition number of the preconditioned covariance matrix is 4.2, which is much less than the condition number of the original covariance matrix 77.1. It is seen from Fig. 8 that only 5 iterations are needed in PCG-PMF to reach a relative approximation error under 1%, while 20 iterations are needed for CG-PMF.

Our next example considers the adaptive PAMF detector, for which the disturbance covariance matrix is unknown and the sample covariance matrix is estimated by (52). Similar to the PMF detector, we compare two implementations of the PAMF detector, including the DMI-PAMF and CG-PAMF, Here the DMI-PAMF directly inverses the sample covariance matrix to get the maximum-likelihood estimation of AR coefficients [13]. The disturbance is an AR(2) signal, whose disturbance covariance matrix is estimated from $K = 16$ target-free training data vectors, and the AR coefficients are estimated based on the estimated disturbance covariance matrix. The numerical results are shown in Fig. 9. It is observed that both implementations yield an identical detection performance.

The performance of the CG-PAMF with an unknown disturbance AR model order and disturbance covariance matrix is considered next. Both AR model based data and KASSPER 2002 data set are employed in this example. The KASSPER data set was generated by considering practical airborne radar parameters and issues found in a real-world clutter environment [18]. Specifically, the simulated airborne radar platform travels at a speed of 100 m/s with a 3° crab angle. The radar carrier frequency is 1240 MHz. The horizontal 11 antenna elements form a ULA with a spacing of 0.1092 m between adjacent elements, and the transmit array is uniformly weighted and phased to steer the mainbeam to 195°. The pulse repetition frequency is 1984 Hz and a coherent processing interval contains 32 pulses. Only the first 8 elements are used in our simulation. We use the covariance matrix associated with range bin 200 in the KASSPER data set to generate the test data and the covariance matrices from the neighboring ranges bins to generate the training signals. A target is injected into the test cell with a normalized spatial frequency 0.1 and a normalized Doppler frequency 0.35.

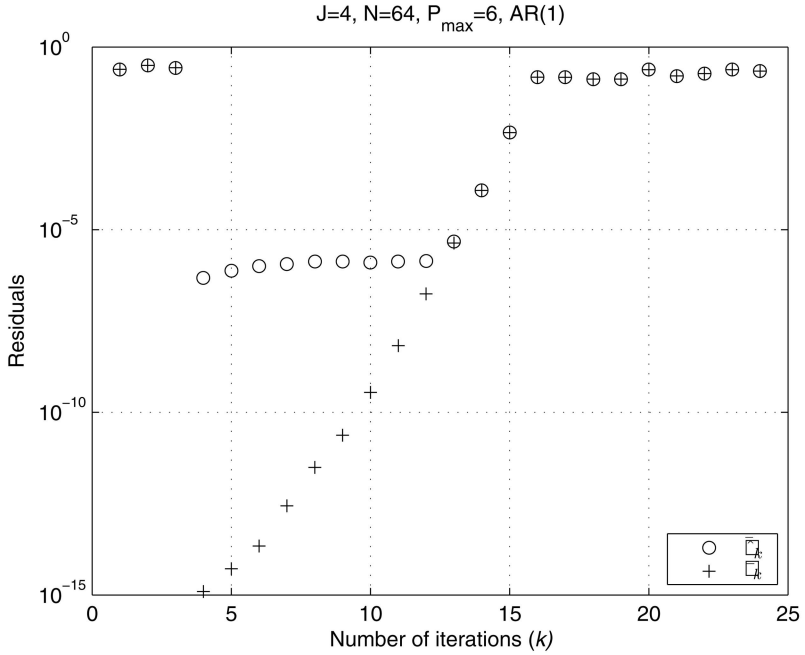

Fig. 4. Residuals $\bar{\epsilon}_{J_p}$ and $\bar{\hat{\epsilon}}_{J_p}$ for model order selection in CG-PMF ($J = 4$; $N = 64$; $P = 1$; $\bar{P} = 6$).

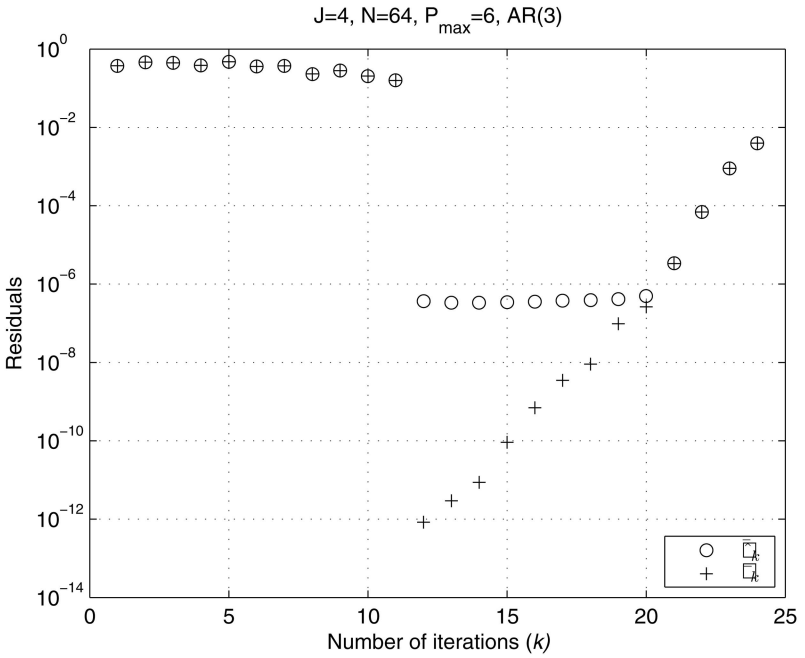

Fig. 5. Residuals $\bar{\epsilon}_{J_p}$ and $\bar{\hat{\epsilon}}_{J_p}$ for model order selection in CG-PMF ($J = 4$; $N = 64$; $P = 3$; $\bar{P} = 6$).

The numerical results are shown in Fig. 10 for the AR model based data and, respectively, Fig. 11 for the KASSPER 2000 data, where OSCG-PAMF (unknown P) represents the CG-PAMF detector with the CG-based model order selection method which employs a model order upper bound $\bar{P}$ calculated by (33). In Fig. 11 we also include for comparison the joint domain localized (JDL) detector [20], a popular reduced-dimensional STAP solution in scenarios of limited training. The JDL is implemented by using 3 beams and 3 Doppler bins for adaptivity. It is seen that the performance of the OSCG-PAMF is nearly identical to that of CG-PAMF with known P (AR data) or a preselected $P = 2$ (KASSPER data). For the case of AR data, we noticed that only one model order selection error ($\hat{P} \neq P$) occurred out of 20000 simulations. Moreover, using the relevant parameters of the KASSPER data, we have $\beta = 2v_{\mathrm{g}}T_{\mathrm{r}}/d = 0.923$. It follows that for $J = 8$ elements, the maximum number of CG iterations needed by the CG-PAMF

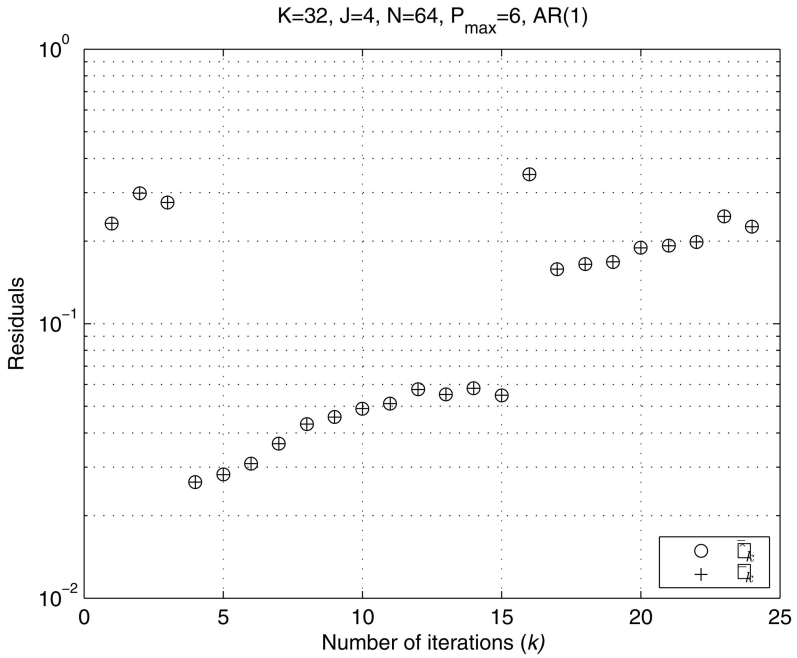

Fig. 6. Residuals $\bar{\epsilon}_{Jp}$ and $\bar{\hat{\epsilon}}_{Jp}$ for model order selection in CG-PAMF ($K = 32$; $J = 4$; $N = 64$; $P = 1$; $\bar{P} = 6$).

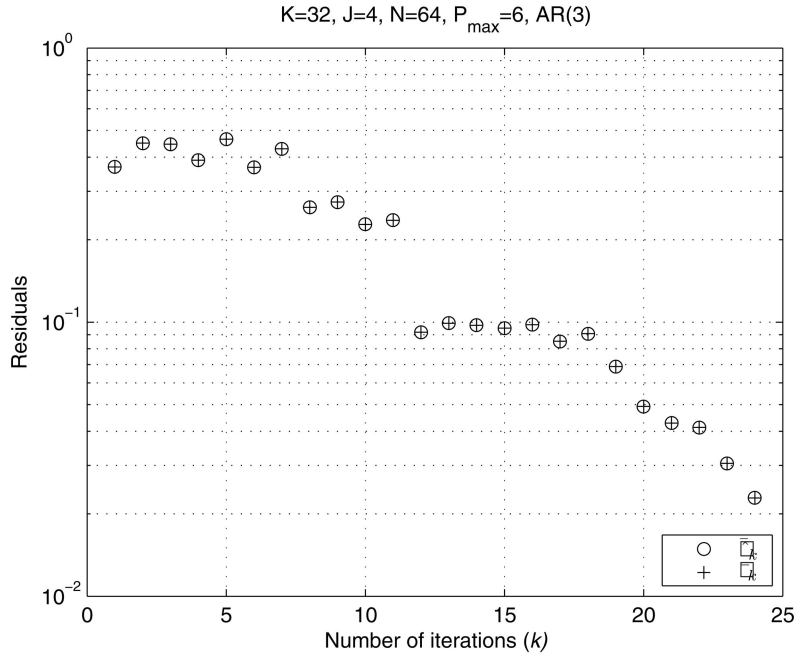

Fig. 7. Residuals $\bar{\epsilon}_{Jp}$ and $\bar{\hat{\epsilon}}_{Jp}$ for model order selection in CG-PAMF ($K = 32$; $J = 4$; $N = 64$; $P = 3$; $\bar{P} = 6$).

for a given model order p is estimated to be $r_{cp} + 1 = \lceil 8.077 + 0.923p \rceil$. For example, the maximum numbers of CG iterations for $p = 2$ is about 10 due to the low-rank structure of the clutter, whereas without such a structure, it would require $pJ = 16$ iterations for the CG to converge. It is also seen in Fig. 11 that the PAMF detectors outperform the JDL-AMF detector. The JDL-AML experiences a loss of about 4 dB compared with the MF.

Finally, we compare the complexity in terms of the number of flops required by the CG and DMI implementations. The flops required by the CG-PAMF and DMI-PAMF versus the AR model order p are shown in Fig. 12. For the DMI-PAMF, the QR decomposition is adopted to get the J-channel AR coefficients. It is seen that the complexity of the CG-PAMF is lower than that of the DMI-PAMF.

VII. CONCLUSIONS

The CG algorithm was employed to solve the linear prediction problem underlying the PMF and PAMF detectors. It is shown that the CG algorithm

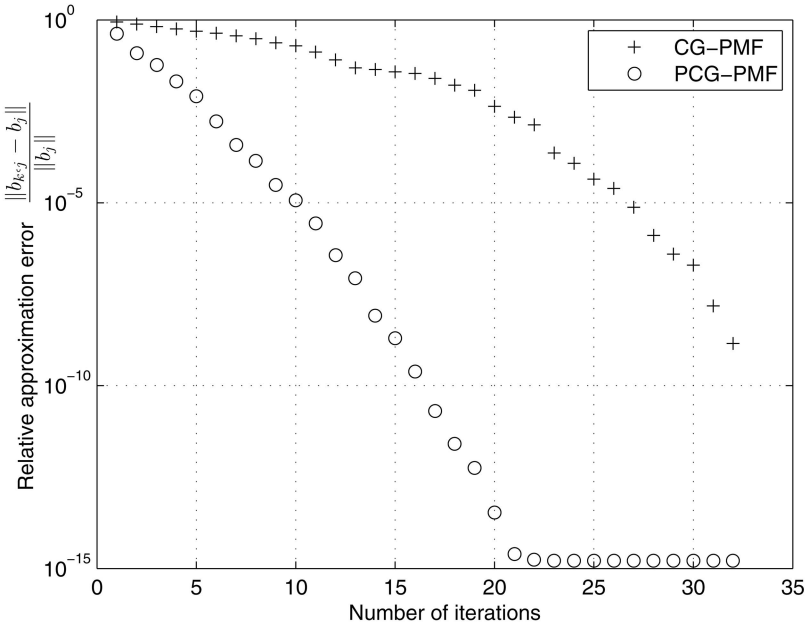

Fig. 8. Convergence of CG-PMF and PCG-PMF ($J = 4$; $P = 8$).

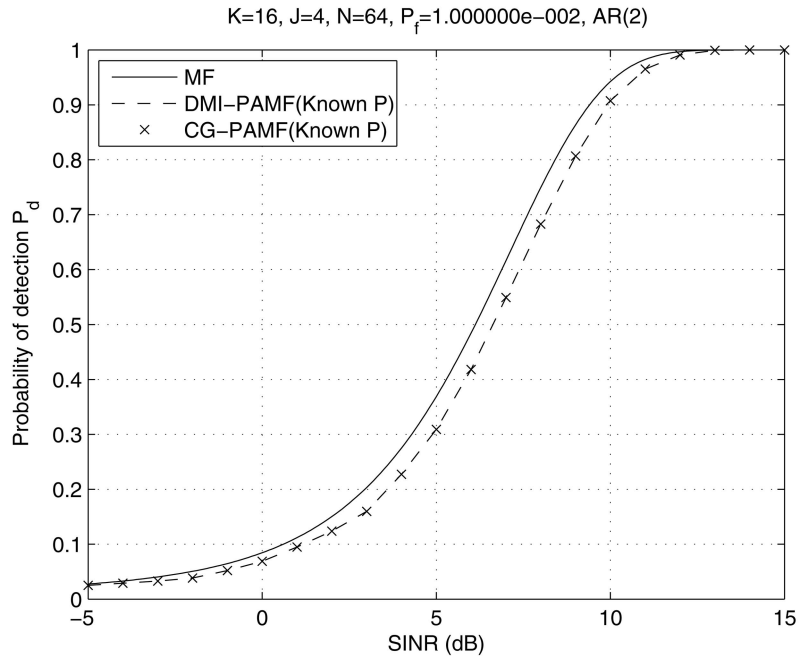

Fig. 9. Probability of detection versus SINR of PAMF for AR data($K = 16$; $J = 4$; $N = 64$; $P = 2$).

leads to not only new efficient implementations, but also new insights of these parametric detectors as reduced-dimensional subspace detectors. In particular, the linear prediction filter and whitening filter of the PMF and PAMF detectors are within the Krylov subspace of dimension JP, and these detectors are reduced JP-dimensional subspace detectors, where J and P are the number of channels and AR model order, respectively. We examined the convergence rate of the CG parametric detectors. In airborne radar applications, the special low-rank structure of the disturbance covariance matrix implies that a rapid convergence is possible, whereby convergence can be achieved without completing a full round of CG iterations. Even for disturbance covariance matrices that do not have the low-rank structure, preconditioning methods can be used to speed up the convergence rate. In general, the CG parametric detectors are more efficient than their counterparts implemented in conventional approaches. We also presented a new CG-based AR model order selection method, which is naturally integrated

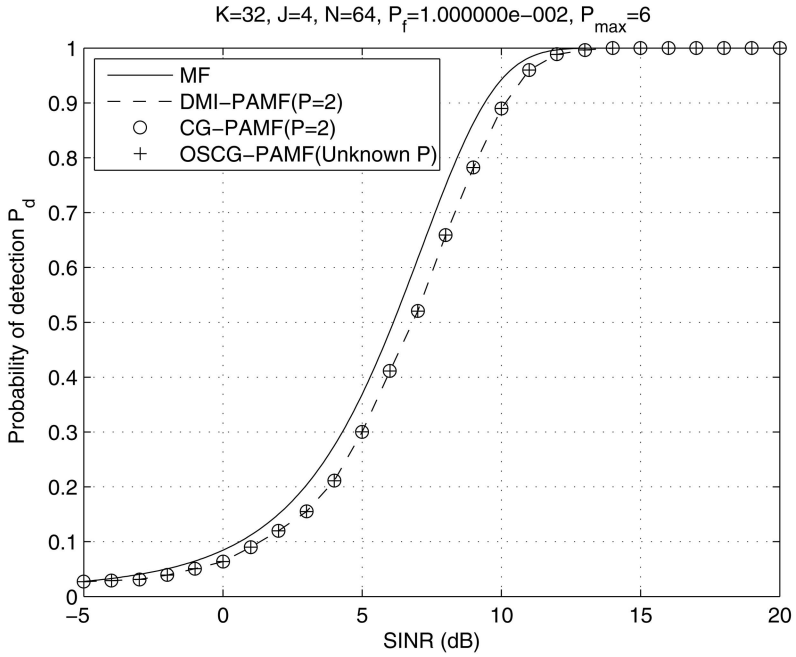

Fig. 10. Probability of detection versus SINR for AR data ($K = 32$; $J = 4$; $N = 64$; $P = 2$; $\bar{P} = 6$).

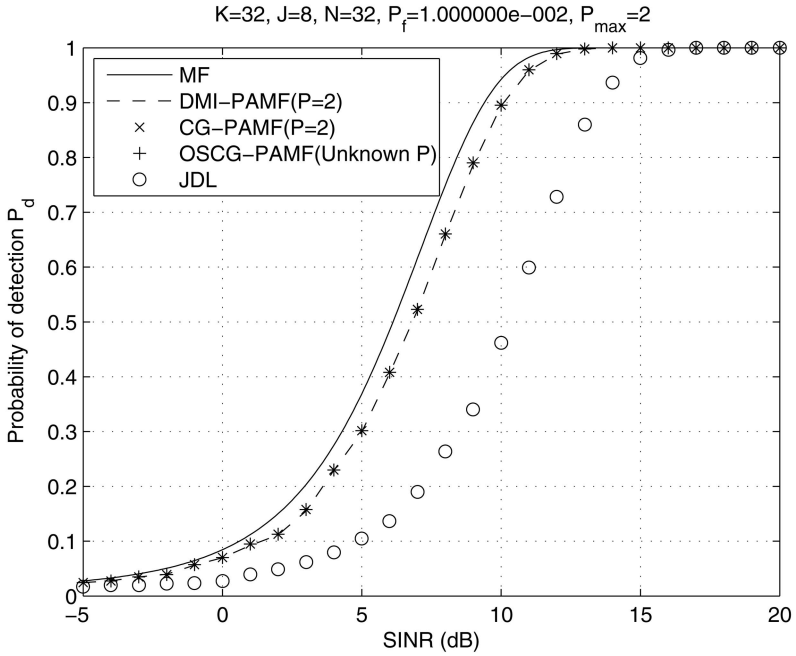

Fig. 11. Probability of detection versus SINR for KASSPER 2002 data ($K = 32$; $J = 8$; $N = 32$; $P = 2$; $\bar{P} = 2$).

with the CG iterations. The proposed techniques are illustrated by using both KASSPER and other simulated data.

Finally, we note that the CG algorithm bears some similarity to a vector space approach [21] to solving the multi-dimensional Yule-Walker equation for an arbitrary region of support. Both involve the use of conjugate orthogonal basis vectors. A future subject would be to investigate the relation of the two approaches and explore the application of the CG algorithm for multi-dimensional and multichannel applications.

APPENDIX I. PROOF OF LEMMA 1

It is well known that the conjugate-direction vectors obtained by the CG algorithm solving the Wiener-Hopf equation (28) span the Krylov subspace [7]:

$$\mathcal{K}(\mathbf{R}_j^{(\bar{P})}, \mathbf{R}_{\mathbf{y}}^{(\bar{P})}, k) = \text{span}\{\mathbf{D}_{1,j}^{(\bar{P})}, \mathbf{D}_{2,j}^{(\bar{P})}, \ldots, \mathbf{D}_{k,j}^{(\bar{P})}\}. \quad (56)$$

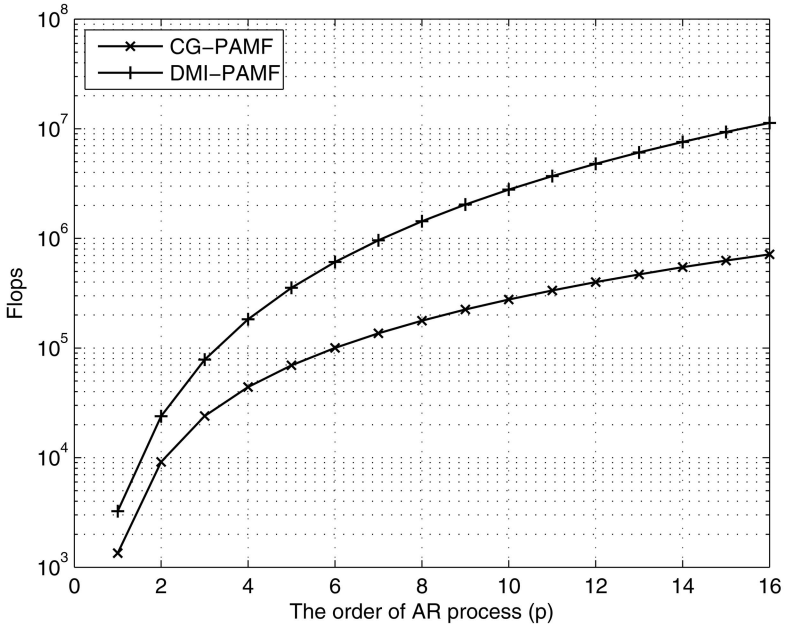

Fig. 12. Computational complexity of CG-PAMF and DMI-PAMF versus AR model order p ($K = 32$; $J = 8$; $N = 32$).

Furthermore, the truncated solution obtained at the kth iteration $\mathbf{B}_{k,j}^{(\bar{P})}$ minimizes the $\mathbf{R}_{\mathbf{y}}^{(\bar{P})}$-norm of the approximation error over all vectors on $\mathcal{K}(\mathbf{R}_j, \mathbf{R}_{\mathbf{y}}^{(\bar{P})}, k)$ [22], i.e.,

$$\|\mathbf{B}_j^{(\bar{P})} - \mathbf{B}_{k,j}^{(\bar{P})}\|_{\mathbf{R}_{\mathbf{y}}^{(\bar{P})}} = \min_{a_k} \left\| \mathbf{x} - \sum_{k=0}^{r} a_k \mathbf{R}_{\mathbf{y}}^{(\bar{P})k} \mathbf{B}_j^{(\bar{P})} \right\|_{\mathbf{R}_{\mathbf{y}}^{(\bar{P})}}. \tag{57}$$

Therefore, the truncated solution obtained at the kth iteration $\mathbf{B}_{k,j}^{(\bar{P})}$ is the $\mathbf{R}_{\mathbf{y}}^{(\bar{P})}$-orthogonal projection of the Wiener solution $\mathbf{B}_j^{(\bar{P})}$ to the subspace $\mathcal{K}(\mathbf{R}_j, \mathbf{R}_{\mathbf{y}}^{(\bar{P})}, k)$, and $\boldsymbol{\alpha}_{k,j} = [\alpha_{1,j}^{(\bar{P})}, \alpha_{2,j}^{(\bar{P})}, \ldots, \alpha_{k,j}^{(\bar{P})}]^{\mathrm{T}}$ contains the coordinate values of conjugate-direction vectors $\{\mathbf{D}_{1,j}^{(\bar{P})}, \mathbf{D}_{2,j}^{(\bar{P})}, \ldots, \mathbf{D}_{k,j}^{(\bar{P})}\}$, which are given by

$$\alpha_{k,j}^{(\bar{P})} = \frac{\mathbf{D}_{k,j}^{(\bar{P})H} \mathbf{R}_{\mathbf{y}}^{(\bar{P})} \mathbf{B}_j^{(\bar{P})}}{\mathbf{D}_{k,j}^{(\bar{P})H} \mathbf{R}_{\mathbf{y}}^{(\bar{P})} \mathbf{D}_{k,j}^{(\bar{P})}}. \tag{58}$$

With the definition of $\tilde{\mathbf{D}}_{k,j}$ by (30), we can write after JP iterations

$$\boldsymbol{\alpha}_{JP,j} = \tilde{\mathbf{D}}_{JP,j}^{\mathrm{H}} \mathbf{B}_j^{(\bar{P})} \tag{59}$$

where $\tilde{\mathbf{D}}_{JP,j} = [\tilde{\mathbf{D}}_{1,j}, \tilde{\mathbf{D}}_{2,j}, \ldots, \tilde{\mathbf{D}}_{JP,j}]$. Recalling $\mathbf{B}_j^{(\bar{P})} = [\mathbf{B}_j^{\mathrm{T}}, \mathbf{0}_{J(\bar{P}-P)\times 1}^{\mathrm{T}}]^{\mathrm{T}}$, we have

$$\boldsymbol{\alpha}_{JP,j} = [\bar{\mathbf{D}}_{JP,j}^{\mathrm{H}} \quad \tilde{\mathbf{D}}_{JP,\mathrm{d}}^{\mathrm{H}}] \begin{bmatrix} \mathbf{B}_j \\ \mathbf{0} \end{bmatrix} \tag{60}$$

where $\bar{\mathbf{D}}_{JP,j} \in \mathbb{C}^{JP \times JP}$ is the upper $JP \times JP$ block matrix of $\tilde{\mathbf{D}}_{JP,j}$, and $\tilde{\mathbf{D}}_{JP,\mathrm{d}}$ contains the lower block of $\tilde{\mathbf{D}}_{JP,j}$. Then $\mathbf{B}_j$ is given by

$$\mathbf{B}_j = \bar{\mathbf{D}}_{JP,j}^{-H} \boldsymbol{\alpha}_{JP,j}. \tag{61}$$

The intermediate solution obtained at the JPth CG iteration is

$$\mathbf{B}_{JP,j}^{(\bar{P})} = \sum_{m=1}^{JP} \alpha_{m,j} \mathbf{D}_{m,j}^{(\bar{P})} = \mathbf{D}_{JP,j}^{(\bar{P})} \boldsymbol{\alpha}_{JP,j}. \tag{62}$$

It follows from (61) and (62) that $\mathbf{B}_{JP,j}^{(\bar{P})}$ and $\mathbf{B}_j$ are related by

$$\mathbf{B}_{JP,j}^{(\bar{P})} = \mathbf{D}_{JP,j}^{(\bar{P})} \bar{\mathbf{D}}_{JP,j}^{\mathrm{H}} \mathbf{B}_j = \mathbf{W}_{JP,j} \mathbf{B}_j \tag{63}$$

where $\mathbf{W}_{JP,j} = \mathbf{D}_{JP,j}^{(\bar{P})} \bar{\mathbf{D}}_{JP,j}^{\mathrm{H}} \in \mathbb{C}^{J\bar{P} \times JP}$, which completes the proof.

REFERENCES

[1] Ward, J.
Space-time adaptive processing for airborne radar.
Lincoln Laboratory, MIT, Technical Report 1015, Dec. 1994.

[2] Brennan, L. E. and Reed, I. S.
Theory of adaptive radar.
IEEE Transactions on Aerospace and Electronic Systems, **AES-9**, 2 (1973), 237–252.

[3] Robey, F. C.
A CFAR adaptive matched filter detector.
IEEE Transactions on Aerospace and Electronic Systems, **28**, 1 (Jan. 1992), 208–216.

[4] Kelly, E. J.
An adaptive detection algorithm.
IEEE Transactions on Aerospace and Electronic Systems, **22**, 1 (Mar. 1986), 115–127.

[5] Rangaswamy, M. and Michels, J. H.
A parametric multichannel detection algorithm for correlated non-Gaussian random processes.
In *Proceedings of the 1997 IEEE National Radar Conference*, Syracuse, NY, May 1997, 349–354.

[6] Román, J. R., et al.
Parametric adaptive matched filter for airborne radar applications.
IEEE Transactions on Aerospace and Electronic Systems, **36**, 2 (Apr. 2000), 677–692.

[7] Golub, G. H. and Van Loan, C. F.
Matrix Computations (3rd ed.).
Baltimore, MD: The Johns Hopkins University Press, 1996.

[8] Chan, T. and Olkin, J.
Circulant preconditioners for Toeplitz-block matrices.
Numerical Algorithms, **6**, 1 (Mar. 1994), 89–101.

[9] Jin, X-Q.
Developments and Applications of Block Toeplitz Iterative Solvers.
Norwell, MA: Kluwer Academic Publishers, 2002.

[10] Reed, I. S., Mallett, J. D., and Brennan, L. E.
Rapid convergence rate in adaptive arrays.
IEEE Transactions on Aerospace and Electronic Systems, **AES-10**, 6 (1974), 853–863.

[11] Van Trees, H. L.
Detection, Estimation, and Modulation Theory, Part I.
Hoboken, NJ: Wiley, 1968.

[12] Sohn, K. J., Li, H., and Himed, B.
Parametric Rao test for multichannel adaptive signal detection.
IEEE Transactions on Aerospace and Electronic Systems, **43**, 3 (July 2007), 920–933.

[13] Kay, S. M.
Modern Spectral Estimation: Theory and Application.
Upper Saddle River, NJ: Prentice-Hall, 1988.

[14] Haimovich, A.
The eigencanceler: Adaptive radar by eigenanalysis methods.
IEEE Transactions on Aerospace and Electronic Systems, **32**, 2 (Apr. 1996), 532–542.

[15] Chan, T.
An optimal circulant preconditioner for Toeplitz systems.
SIAM Journal on Scientific and Statistical Computing, **9** (1988), 766–771.

[16] Vescovo, R.
Inversion of block-circulant matrices and circular array approach.
IEEE Transactions on Antennas and Propagation, **45**, 10 (Oct. 1997), 1565–1567.

[17] Chan, R. H. and Ng, M. K.
Conjugate gradient methods for Toeplitz systems.
SIAM Review, **38**, 3 (Sept. 1996), 427–482.

[18] Bergin, J. S. and Techau, P. M.
High-fidelity site-specific radar simulation: KASSPER'02 workshop datacube.
Information Systems Laboratories, Inc., Vienna, VA, Technical Report ISL-SCRD-TR-02-105, May 2002.

[19] Michels, J. H., Roman, J. R., and Himed, B.
Beam control using the parametric adaptive matched filter stap approach.
In *Proceedings of 2003 IEEE Radar Conference*, Huntsville, AL, May 2003, 405–412.

[20] Wang, H. and Cai, L.
On adaptive spatial-temporal processing for airborne surveillance radar systems.
IEEE Transactions on Aerospace and Electronic Systems, **30**, 3 (July 1994), 660–670.

[21] Kay, S. and Carbone, C.
Vector space solution to the multidimensional Yule-Walker equations.
In *Proceedings of the International Conference on Acoustics, Speech, and Signal Processing*, vol. 3, Hong Kong, Apr. 2003, 289–292.

[22] Saad, Y.
Iterative Methods for Sparse Linear Systems.
Society for Industrial and Applied Mathematics, Philadelphia, PA, 2003.

Chaoshu Jiang (M'11) was born in China in 1973. He received the B.S., M.S., and Ph.D. degrees in electronic engineering from University of Electronic Science and Technology of China, in 1996, 1999, and 2006, respectively.

From 1999 to 2000 he worked in ZTE Corporation as a hardware engineer. Since 2000, he has been with the School of Electronic Engineering, University of Electronic Science and Technology of China, Chengdu City, Sichuan Province, China, where he is currently an associate professor. From 2007 to 2009, he worked as a post-doc in the Second Research Institute of Civil Aviation Administration of China (CAAC) on technology of airport surface surveillance. From 2009 to 2010, he worked in Stevens Institute of Technology as a post-doc on signal detection.

Dr. Jiang received the 2009 advanced science and technology award of CAAC in 2010.

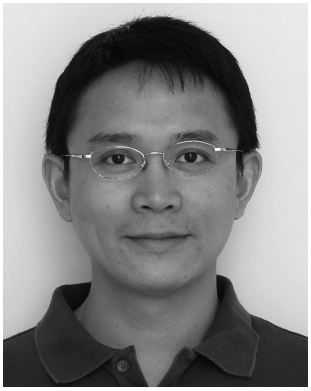

Hongbin Li (M'99—SM'09) received the B.S. and M.S. degrees from the University of Electronic Science and Technology of China, Chengdu, in 1991 and 1994, respectively, and the Ph.D. degree from the University of Florida, Gainesville, in 1999, all in electrical engineering.

From July 1996 to May 1999, he was a research assistant in the Department of Electrical and Computer Engineering at the University of Florida. He was a summer visiting faculty member at the Air Force Research Laboratory in the summers of 2003, 2004, and 2009. Since July 1999, he has been with the Department of Electrical and Computer Engineering, Stevens Institute of Technology, Hoboken, NJ, where he is a professor. His current research interests include statistical signal processing, wireless communications, and radars.

Dr. Li is a member of Tau Beta Pi and Phi Kappa Phi. He received the Harvey N. Davis Teaching Award in 2003 and the Jess H. Davis Memorial Award for excellence in research in 2001 from the Stevens Institute of Technology, and the Sigma Xi Graduate Research Award from the University of Florida in 1999. He is presently a member of both the Sensor Array and Multichannel (SAM) Technical Committee and the Signal Processing Theory and Methods (SPTM) Technical Committee of the IEEE Signal Processing Society. He has been an editor or associate editor for the *IEEE Transactions on Wireless Communications*, *IEEE Signal Processing Letters*, and *IEEE Transactions on Signal Processing*, and served as a guest editor for *EURASIP Journal on Applied Signal Processing*, Special Issue on Distributed Signal Processing Techniques for Wireless Sensor Networks.

Muralidhar Rangaswamy (S'89—M'93—SM'98—F'06) received the B.E. degree in electronics engineering from Bangalore University, Bangalore, India in 1985 and the M.S. and Ph.D. degrees in electrical engineering from Syracuse University, Syracuse, NY, in 1992.

He is presently employed as a principal electronics engineer and technical advisor for the RF Exploitation Technology Branch at the Sensors Directorate of the Air Force Research Laboratory (AFRL), Wright Patterson Air Force Base, OH. Prior to this he has held industrial and academic appointments. His research interests are in the areas of radar phenomenology and radar signal processing.

Dr. Rangaswamy has authored or coauthored more than 120 refereed journal articles and conference record papers in the areas of his research interests. Additionally, he is a contributor to 5 book chapters and a coinventor on 3 U.S. patents. He received the Fred Nathanson Memorial Outstanding Young Radar Engineer Award from the IEEE AESS in 2005, the Distinguished Member Award from the IEEE Boston Section in 2006 and the IEEE Region 1 award in 2007 for technical contributions to radar. He received the 2005 Charles Ryan Memorial Basic Research Award from the Sensors Directorate at AFRL as well as 40 AFRL scientific achievement awards. He is a member of the Radar Systems Panel within the IEEE AESS. He serves as the technical editor (associate editor-in-chief) for radar systems within the *IEEE Transactions on Aerospace and Electronic Systems*. He is an adjunct professor at the School of Electrical and Computer Engineering at Purdue University.